Journal of Sea Research 95 (2015) 1–15

Contents lists available at ScienceDirect

Journal of Sea Research

journal homepage: www.elsevier.com/locate/seares

# Intrusion of the Pearl River plume into the main channel of the Taiwan Strait in summer

Yan Bai [a,*], Ting-Hsuan Huang [b], Xianqiang He [a,d], Shu-Lun Wang [g], Yi-Chia Hsin [f], Chau-Ron Wu [c], Weidong Zhai [e], Hon-Kit Lui [b], Chen-Tung Arthur Chen [a,b,d]

[a] State Key Laboratory of Satellite Ocean Environment Dynamics, Second Institute of Oceanography, State Oceanic Administration, Hangzhou, China
[b] Department of Oceanography, National Sun Yat-sen University, Kaohsiung, Taiwan
[c] Department of Earth Sciences, National Taiwan Normal University, Taipei, Taiwan
[d] Department of Ocean Science and Engineering, Zhejiang University, Hangzhou, China
[e] State Key Laboratory of Marine Environmental Science, Xiamen University, Xiamen, China
[f] Research Center for Environmental Changes, Academia Sinica, Taipei, Taiwan
[g] Department of Marine Environmental Engineering, National Kaohsiung Marine University, Kaohsiung, Taiwan

ARTICLE INFO

*Article history:*
Received 11 February 2013
Received in revised form 30 September 2014
Accepted 1 October 2014
Available online 12 October 2014

*Keywords:*
Pearl River plume
Taiwan Strait
Penghu Channel
Satellite observations

ABSTRACT

The Penghu Channel is the main channel connecting the East and South China Seas, two of the largest marginal seas in the world. Located in the southeast of Taiwan Strait, the Penghu Channel is usually covered by the high salinity water from the South China Sea and the Kuroshio. However, we observed abnormal low-salinity water in the Penghu Channel during a cruise through the southern Taiwan Strait and northern South China Sea in August 2008. We argue that the normalized alkalinity is a good indicator for the identification of a river plume as it is not affected by rainwater. Using satellite-derived water transparency and chlorophyll images and field-measured alkalinity, the source of this low salinity water was found to be the intrusion of the Pearl River plume. A significant phytoplankton bloom across the entire Taiwan Strait occurred with the intrusion event. The intrusion was not a unique event, as we also found a strong jet-shaped Pearl River plume intruding into the Penghu Channel in the summer of 2009 from cloud-free satellite-derived images. Time series satellite data reveal that the Pearl River plume intrudes into the Penghu Channel in the summer of most years. Multiple data analysis and modeling simulation indicate that a large river discharge and strong southwesterly winds on the shelf may be responsible for the significant intrusion of the Pearl River plume into the Penghu Channel in summer. As the Pearl River plume has a high nutrient and dissolved inorganic carbon content, combined with the strong northward flows through the Penghu Channel, such intrusions may contribute to the nutrient dynamics and carbon budget of the East and northern South China Seas.



## 1. Introduction

The South China Sea (SCS) and the East China Sea (ECS) are the two main marginal seas in the western Pacific Ocean, and are ranked as the second and eleventh largest marginal seas in the world, respectively. The SCS and ECS are connected by the Taiwan Strait (TWS), which is about 180 km wide and 350 km long, with an average depth of about 60 m (Jan et al., 2002), as shown in Fig. 1. The current through the TWS has a direct impact on the circulation and biogeochemical processes in the SCS, the ECS and even the Japan Sea (Chen and Wang, 1999; Hong et al., 2011a; Isobe, 1999; Katoh et al., 2000; Liu et al., 2000).

Circulation in the TWS is mainly controlled by the strong East Asia monsoon and the complex topography of the Strait (Hong et al., 2011a; Naik and Chen, 2008; Tseng and Shen, 2003). In winter, the Zhejiang–Fujian Coastal Current flows southward along the eastern coast of China, but the direction of the current on the eastern side of the TWS is still not well defined (Chen and Sheu, 2006; Chen and Wang, 1999; Wu and Hsin, 2005). In summer, it is generally accepted that the entire TWS is dominated by a northward current driven by southwesterly winds, except during typhoon events (Chen et al., 2003; He et al., 2014; Hsin et al., 2010). Separated by the shallow Taiwan Bank located in the middle of the southern TWS, the northward currents in the southern TWS are divided into a two-pronged flow. The eastern prong flows through the Penghu Channel and is made up of oligotrophic waters from the SCS and the Kuroshio, whereas the western prong flows through the channel between mainland China and the Taiwan Bank and derives from the upwelling of the SCS subsurface water and coastal water (Hong et al., 2009, 2011b). It is well known that the deep Penghu Channel is the main pathway for volume transport through the Strait in summer because of the topography of the TWS (Jan and Chao, 2003; Jan et al., 2002; Wu et al., 2007).

* Corresponding author. Tel.: +86 571 81963119; fax: +86 571 81963112.
*E-mail address:* baiyan_ocean@126.com (Y. Bai).

http://dx.doi.org/10.1016/j.seares.2014.10.003
1385-1101/

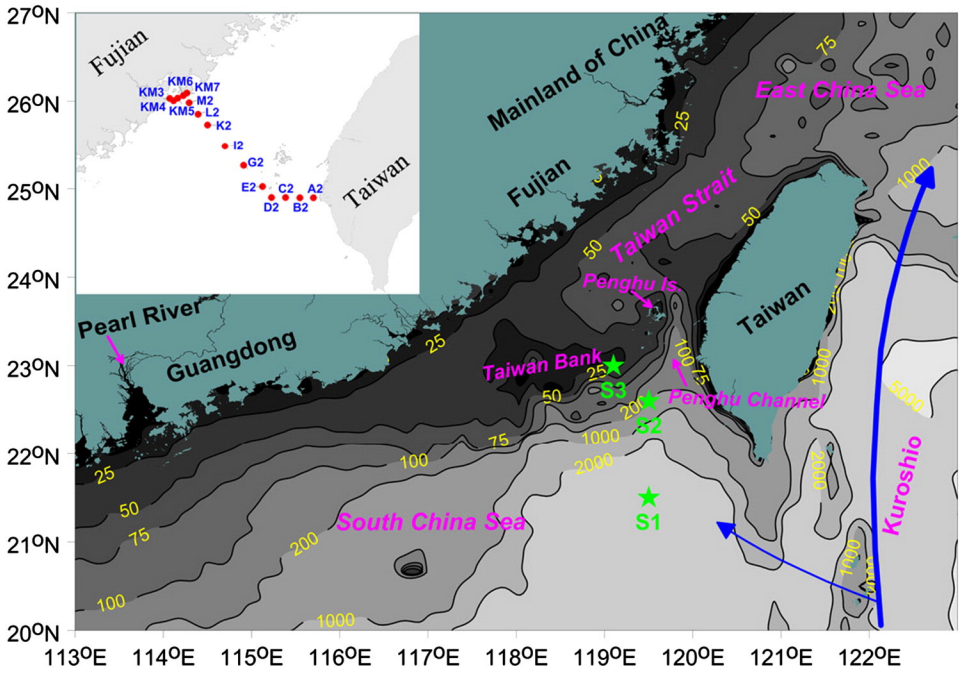


**Fig. 1.** Location and bathymetry (isobaths in meters) of the study area. Also shown are the sampling stations along the southern Taiwan Strait transect of the ORI-873 cruise in 2008 (upper left panel). Star symbols of S1, S2, and S3 are the locations of three selected points to show the variation of time series satellite data during 2000–2010 (shown in Fig. 9).

Flowing into the northern SCS, the Pearl River is the largest river which inputs into the northward currents in TWS. As the largest river in China after the Yangtze River and the 13th largest river in the world in terms of freshwater discharge (Yin et al., 2004), the Pearl River delivers $3.5 \times 10^{11}$ $m^3$/yr of freshwater and $85 \times 10^6$ tons/yr of sediment load into the SCS. The Pearl River has about 80% of the discharge occurring during the wet season of April–September and only 20% during the dry season of October–March (Yin et al., 2004; Zhang et al., 1999). The annual-mean discharge of the Pearl River is 10,524 $m^3$/s, and the maximum river discharge occurs in July (Yin et al., 2004). The water comes from three main branches – the Dong Jiang (East River), Xi Jiang (West River) and Bei Jiang (North River) – before entering the SCS. The general pathway of the Pearl River plume (PRP) is well defined, and is mainly driven by the East Asia Monsoon (Dong et al., 2004). During the dry season, with strong northeasterly winds and low river discharge, the plume is advected westward by coastal current induced by the northeasterly wind, and the horizontal extent of the plume is much smaller. However, during the wet season with relative weak southerly winds and a large river discharge, the plume is advected eastward and offshore by the coastal current induced by the upwelling favorable winds (Dong et al., 2004).

Previous studies have found that the PRP could intrude into the southern TWS in summer. Based on the underway measured temperature and salinity at the surface, Chen et al. (2002) observed a 20 km zone with a high temperature (up to 28.6 °C) and low salinity (about 33) extending to the south of the Taiwan Bank. This phenomenon was also found in the summer of 2005, and was confirmed by numerical modeling (Hong et al., 2009). These studies indicate that the PRP and the Yuedong (the eastern Guangdong) Coastal Current, which has a high temperature and a low salinity and density in the upper layer, flow northeastwards through the channel west of the Taiwan Bank (the western prong defined by Hong et al., 2011b). More recently, modeling studies by Gan et al. (2009) and Shu et al. (2011) revealed that the PRP also extends northeastwards to the southern TWS and as far as the southern part of the Penghu Channel. However, these modeling results require validation by satellite and field observations.

During a cruise through the southern TWS and northern SCS in August 2008, we observed water of abnormally low salinity in the Penghu Channel. At the same time, a phytoplankton bloom was observed in the middle and northern TWS from satellite ocean color images. This study aims to trace the source of this low-salinity water to the Pearl River, and to reveal the biological responses to this event through both in-situ measurements and satellite data. To the best of our knowledge, this is the first time that the intrusion of the PRP into the Penghu Channel has been observed by satellite images and confirmed by both modeled results and field data.

## 2. Data and methods

### 2.1. In situ data

The ORI-873 cruise onboard the R/V Ocean Researcher I traversed the northern SCS and the southern TWS from 30 July to 6 August in 2008. The underway salinity and temperature were obtained by a self-recording CTD instrument. The temperature and salinity profiles at each station (Fig. 1) were determined with a shipboard SBE-911-plus conductivity–temperature–depth (CTD) unit manufactured by the Sea-bird Corporation. The temperature was recorded on the 1990 International Temperature Scale and the salinity on the 1978 Practical Salinity Scale. Discrete samples were collected at various depths with a Rosette sampler fitted with 2.5 L Niskin bottles that were mounted on the CTD unit to determine the salinity, pH and titration alkalinity (TA). Data from the sensors on the CTD unit were obtained during both the downcast and the upcast periods. The CTD unit was lowered as well as raised at a rate of about 1.0 m/s. Discrete water samples were taken during the upcast. Salinity in the discrete samples was determined by measuring conductivity with an AUTOSAL salinometer, which was calibrated with IAPSO standard seawater with a precision of 0.003. Values of pH were measured to a precision of ±0.002 at 25 ± 0.05 °C with spectrophotometric seawater pH measurement of m-cresol purple on total scale (Clayton and Byrne, 1993). Total alkalinity was measured using Gran titration (Gran, 1952) composed of an Orion 81-02 pH meter, an Orion 3-Star pH benchtop meter, an 18-ml titration cell and a temperature-controlled water bath set at 25 ± 0.05 °C. The precision of the TA values was ±2–3 μmol/kg, and corrected using Dickson seawater standard as reference. More detailed method descriptions of pH and TA measurements can be referred to Chen and Wang (2006).

### 2.2. Satellite data

Daily satellite images of chlorophyll-a concentration (chla), water transparency, and sea surface temperature (SST) were obtained from the satellite data receiving station of the Second Institute of Oceanography of China (SIO/SOA). The chla and water transparency were retrieved from Aqua/MODIS (the Moderate Resolution Imaging Spectroradiometer) data, while the SST was retrieved from the NOAA-17/AVHRR (Advanced Very High Resolution Radiometer). The water transparency was determined by a semi-analytical algorithm based on the satellite-retrieved chla and suspended particulate matter concentration (He et al., 2004, 2014; Jiao et al., 2007). The spatial resolution of the daily satellite-derived water transparency images is 1′.

We obtained the 8-day composite chla data retrieved by Aqua/MODIS (2002–2010), Terra/MODIS (2000–2010) and SeaWiFS (1998–2010) satellite data from the NASA Ocean Color Website (http://oceancolor.gsfc.nasa.gov). The monthly mean SST retrieved by Terra/MODIS (2000–2010) was also obtained from the NASA ocean color website. The SST is retrieved by the 11 μm band of the Terra/MODIS observed in the daytime. The spatial resolution of the chla and SST datasets is 2.5′ with a global coverage. In addition, we obtained the daily global sea surface wind vector (SSW) data retrieved by QuikSCAT from the NASA Jet Propulsion Laboratory, which has a spatial resolution of 25 km.

### 2.3. Model simulation

The numerical simulations we used are the Seas Around Taiwan (SAT) model (Wu and Hsin, 2012; Wu et al., 2008), which is based on the Princeton Ocean Model. Using the hydrostatic approximation, the SAT model solves three-dimensional primitive equations for the

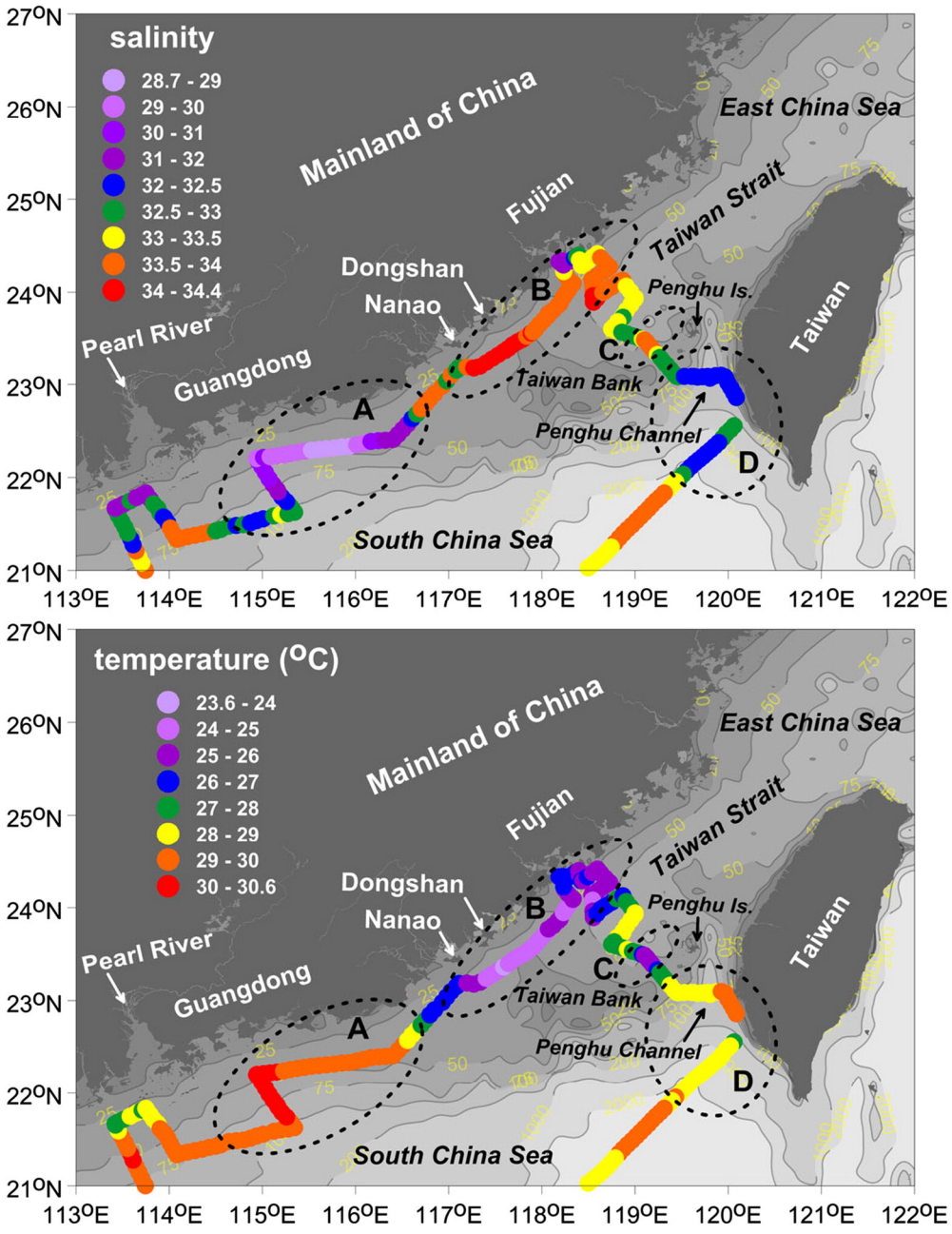


**Fig. 2.** Distributions of the underway surface water salinity and temperature in the southern Taiwan Strait and northern South China Sea as measured on the ORI-873 cruise.

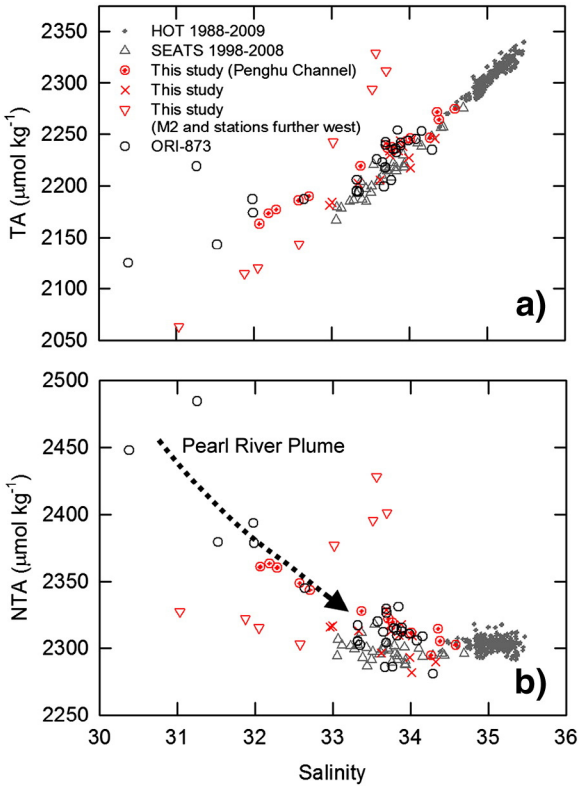


**Fig. 3.** (a) Alkalinity versus salinity and (b) normalized alkalinity versus salinity in surface waters at the HOT and SEATS stations in recent years (taken from Lui and Chen, in preparation), in the cross-section across the southern Taiwan Strait (this study), and Chen's unpublished data off the Pearl River estuary a week before the measurement in the cross-section across the southern Taiwan Strait. The broken arrow shows the flow of the Pearl River plume schematically.

momentum, heat and salt and evaluates turbulence by the 2.5-level Mellor–Yamada scheme. The domain of the SAT model extends zonally from 110.5°E to 126°E and meridionally from 13.8°N to 28°N with a horizontal resolution of 1/20° × 1/20°, and it has 26 sigma levels in the vertical. On open boundaries, the lateral boundary conditions are daily one-way nested to a 1/8° × 1/8° East Asian Marginal Seas (EAMS) model with an expanded domain of 99°E–140°E and 0°–42°N. The SAT and EAMS models we used had been validated carefully with observational data around Taiwan, and used to investigate variations of the current in the Taiwan Strait and the Kuroshio around Taiwan (Hsin et al., 2008, 2010, 2012; Wu and Hsin, 2005, 2012). In this simulation, the model was forced by the 6-hourly 1/4° × 1/4° Cross-Calibrated Multi-Platform (CCMP) Ocean Surface Wind, which was derived through cross-calibration and assimilation of ocean surface wind data from SSM/I, TMI, AMSR-E, SeaWinds on QuikSCAT and SeaWinds on ADEOS-II, and by the 6-hourly 2.5° × 2.5° NCEP-DOE reanalysis II heat flux dataset.

## 3. Results and discussion

### 3.1. Identification of the intrusion of the PRP into the Penghu Channel by field observation

The distributions of the underway measured surface water salinity and temperature in the southern TWS and northern SCS are shown in Fig. 2. In region A, the surface water had a much lower salinity (as low as 29) and a higher temperature (up to 31 °C), indicating the eastward transport of the PRP. In contrast, in region B along the southern Fujian coast, the surface water had a higher salinity (larger than 34) and a lower temperature (less than 26 °C), probably caused by the strong upwelling in this region (Hu et al., 2003). Upwelling was also observed in region C, which had a high salinity and a low temperature but a relatively narrow width. Regions B and C represent two upwelling areas in the southern TWS, one being wind-driven and topographically forced near Dongshan and Nanao in the southwestern TWS, and the other being topographically induced northeast of the Taiwan Bank and southwest of Penghu Island (Hu et al., 2003; Tang et al., 2002). The distributions of the surface water salinity and temperature in regions A, B and C are normal in summer. However, in region D, which is located in the Penghu Channel, the surface water salinity was abnormal and was as low as 32. Normally, the flow through the Penghu Channel is made up of oligotrophic waters from the SCS and the Kuroshio with a surface water salinity of higher than 33.5 (Naik and Chen, 2008). It would thus be of interest to find out the source of the freshwater in the Penghu Channel.

Salinity is arguably one of the most frequently used parameters in identifying a freshwater river plume (e.g. Cooley et al., 2007; Gan et al., 2009, 2010; Hong et al., 2011). However, rain falling off the coast can also make the surface seawater fresher, which makes the plume less identifiable based on a lower salinity level alone. In contrast to river water, rainwater carries little or no alkalinity, especially in the case of the Pearl River, as the basin is widely covered by karst. Consequently, the Pearl River contains a high level of dissolved inorganic carbon, and thus a high level of alkalinity (TA) (Cai et al., 2004; Lou et al., 2014). The average TA just before the various branches of the Pearl

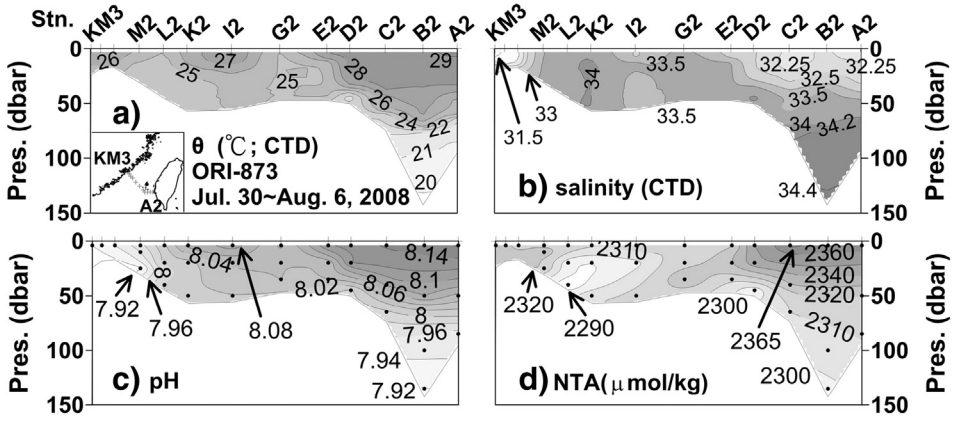


**Fig. 4.** Cross-sectional views of (a) θ, (b) S, (c) pH and (d) NTA from the ORI-873 cruise.

River enter its main estuary is about 1200 μmol/kg at a salinity of less than 0.3 (Chen et al., 2008). In the open ocean, the surface water TA is very predictable, especially in tropical regions because the TA is primarily a function of salinity (Chen and Millero, 1979; Chen and Pytkowicz, 1979; Chen et al., 2006a, 2006b; Lee et al., 2006). Thus, precipitation or evaporation does not affect the normalized alkalinity

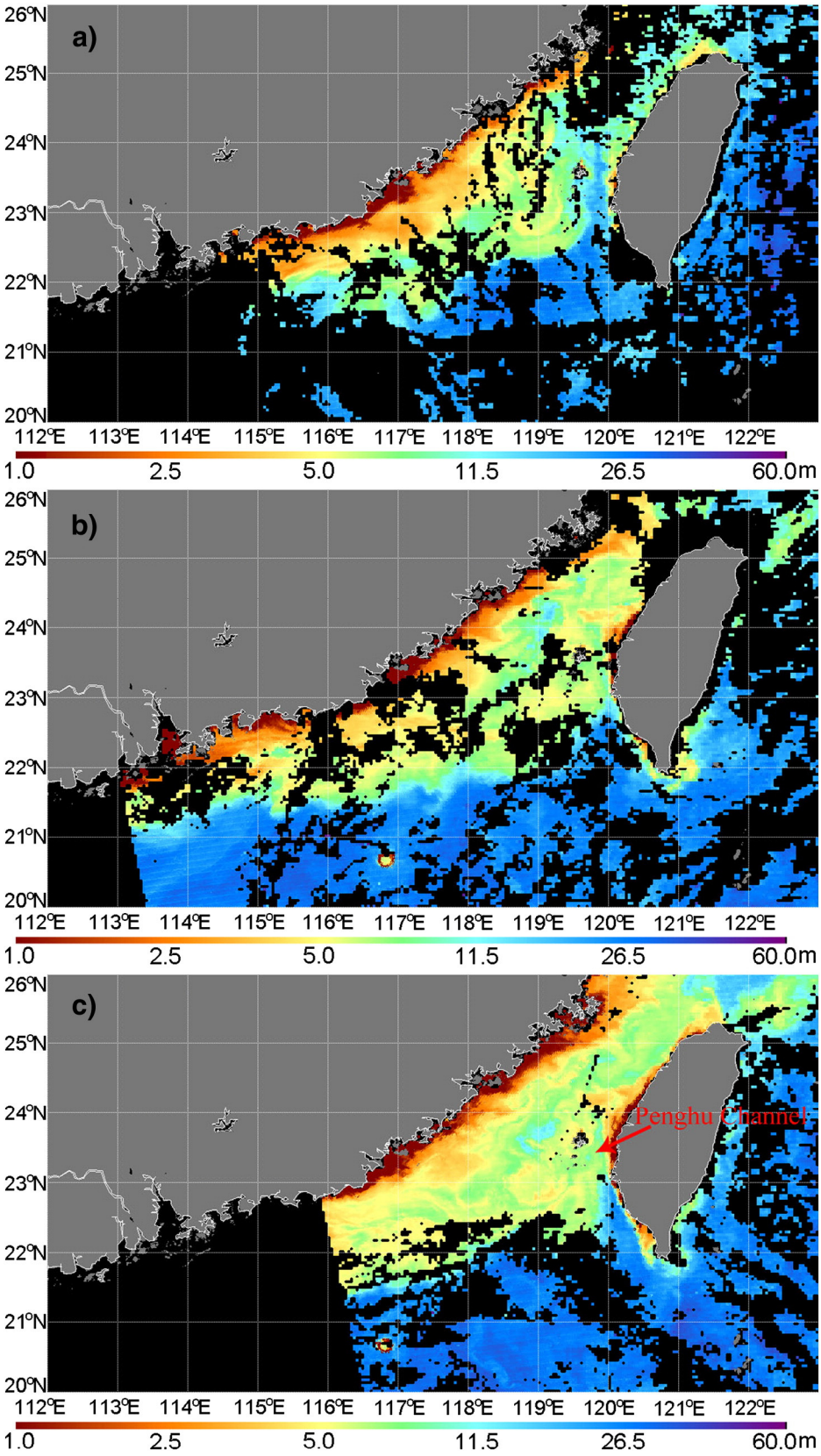


**Fig. 5.** Water transparency images retrieved by MODIS during the intrusion of the PRP into the Penghu Channel. The black regions in the images are covered by cloud or contaminated by sun-glint. (a) 15 July 2008; (b) 22 July 2008; (c) 24 July 2008. (For interpretation of the references to color in the text, the reader is referred to the web version of this article.)

(NTA = TA × 35/S, where S is the measured salinity). As an example, Chen and Pytkowicz (1979) showed that in the entire Pacific Ocean except for the northwest Pacific, the NTA equals 2306 +/− 10 μmol/kg for surface waters with a temperature above 25 °C. More recent TA data from two widely used stations are plotted against salinity in Fig. 3a as another example. The HOT (Hawaii Time Series; data coverage between 1988 and 2009) station is located in the middle of the North Pacific gyre whereas the SEATS (SouthEast Asia Time-Series; data coverage 1998–2008) station is located inside the SCS, yet the TA at both stations covaries linearly with the salinity over the years, and the NTA is 2303 +/− 5.1 μmol/kg (Fig. 3b), which is very close to the value that Chen and Pytkowicz (1979) reported over 30 years ago. Of note is the small standard deviation of this stable NTA value of only slightly higher than the analytical error of 3 μmol/kg (Chen and Wang, 2006), which means that it is relatively easy to identify any disturbances in the NTA.

Although the Pearl River's TA value is only about half of the TA value at the HOT or SEATS stations, the PRP's NTA value is much higher because of the river plume's low salinity. Alkalinity data for the cross-section across the southern Taiwan Strait are also plotted against salinity in Fig. 3a. It is immediately clear that most of the data are higher than the trend for HOT or SEATS stations, especially the surface waters near the Chinese coast (Stn. M2 and stations further west in Fig. 1). Surface waters in the Penghu Channel also fall above the linear TA/S trend (Fig. 3a). Fig. 3b shows the NTA vs. salinity, and the data for the southern Taiwan Strait are again much higher than those from the HOT and SEATS stations. Excluding the four highest values affected by small rivers near the Chinese coast, the highest values of around 2340–2360 μmol/kg are at the surface in the Taiwan Strait in the Penghu Channel. Restated, the NTA for the surface waters at the HOT and SEATS stations is very constant at 2303 ± 5.1 μmol/kg yet the values are as high as 2360 μmol/kg for surface waters in the Penghu Channel. Shown in Fig. 3a and b are also Chen's unpublished data collected off the Pearl River estuary one week before the measurement in the southern Taiwan Strait, and the NTA values as high as 2480 μmol/kg are noted, and these values gradually reduced to 2360 μmol/kg in the Pearl River plume found in the Penghu Channel. Note that we use the traditional normalization method of the TA in this study. Friis et al. (2003) have argued the deficiency of the traditional method to normalize the TA when other factors other than precipitation were in play such as river runoff, and they proposed a salinity adjustment based on a constant and region-specific term for S = 0. Because the purpose of the normalization of the TA in

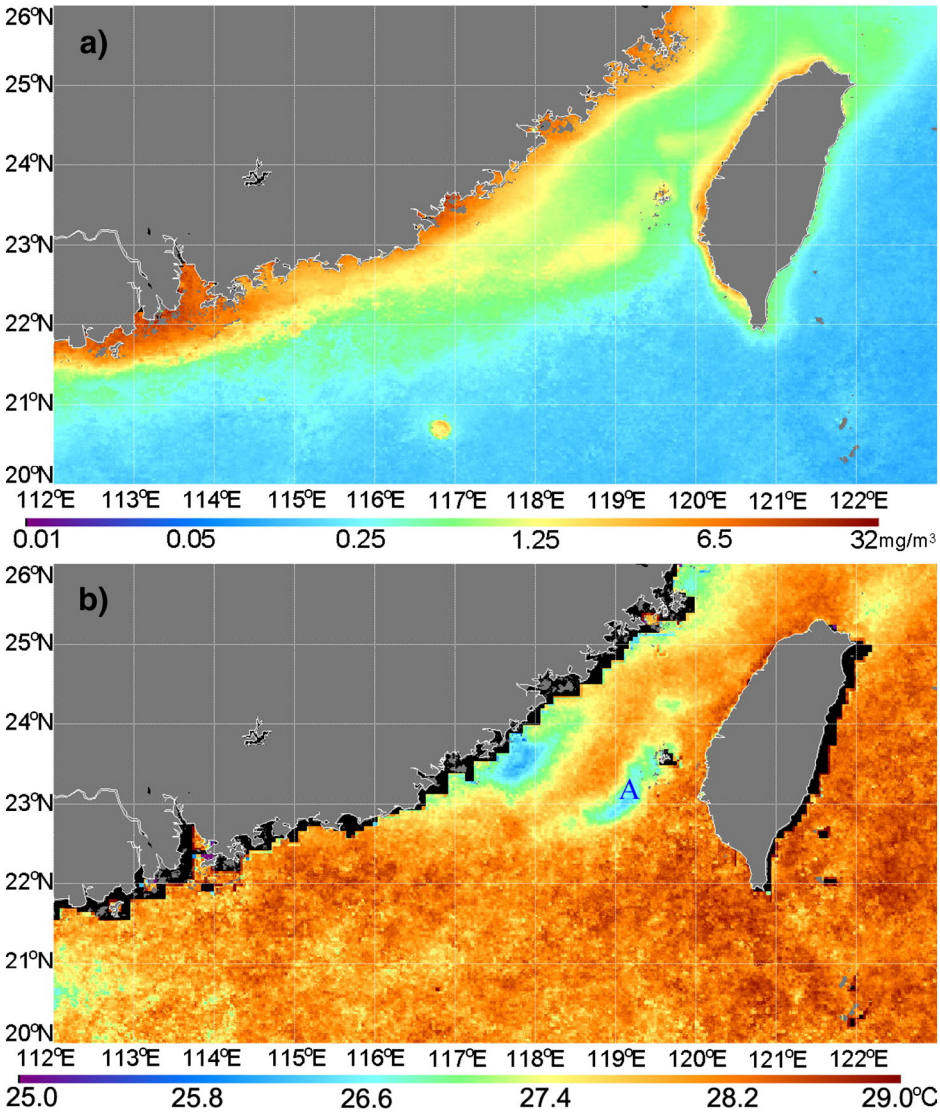


**Fig. 6.** Climatology distributions of the monthly mean chla (a) and SST (b) in July as retrieved by satellite remote sensing.

this study is only to identify the riverine input instead of analyzing the quantitative relationships of NTA and control factors, the effect of the deficiency of traditional normalization method could be ignored.

Another way to show the distribution of the NTA is given in Fig. 4d. Again, the surface waters in the Penghu Channel show distinctively higher values compared to deeper waters in the Channel and further west. These high surface NTA values of 2360 μmol/kg found between Taiwan and Penghu Island (stations A2–C2) in 2008, given in Fig. 4d, are clearly indicative of the riverine influence, which is also in agreement with the satellite water transparency images showing that the PRP extended to east of Penghu Island in that year (Fig. 5). The clean water (shown in blue in Fig. 5a) in the Penghu Channel was replaced by more turbid water (seen in Fig. 5b–c). It is worth noting that the discharge of Taiwanese rivers could also have increased the NTA at station A2 in 2008, but clear water seems to extend northward in the middle of the Penghu Channel and separates any Taiwanese coastal water from waters that have a lower water transparency away from the coast, as can be clearly seen in Fig. 5c. Further, the transect of salinity shown in Fig. 4b clearly shows that the water at station C2 is separated from the water at station A2 by the slightly more saline water at station B2. Thus, the Taiwanese coastal waters with a high NTA only flow along the coast and do not flow westward south of Penghu Island. In addition, although biogeochemical processes such as the formation of pyrite and decalcification of $CaCO_3$ in shallow coastal sediments may increase the alkalinity levels (Brasse et al., 1999; Chen, 1993, 2002; Wang et al., 2000), the high NTA found in surface waters of the Penghu Channel cannot be from bottom sediments as values are higher near the surface rather than near the bottom (Fig. 4d). Fig. 3a clearly demonstrates that the alkalinity values decrease as the salinity decreases, mainly due to dilution effect. To summarize, the NTA data support the satellite observation that the PRP indeed intruded into the Penghu Channel in 2008.

### 3.2. Phytoplankton blooms in the TWS with the intrusion of PRP

Before we present the satellite image of phytoplankton blooms, we first show the climatology distributions of the satellite-derived monthly mean chla and SST data in July in Fig. 6. Near the coasts, chla concentrations are high because of the large amount of nutrients supplied by river runoffs and vertical mixing, even when considering the possibility that the satellite remote sensing may overestimate the chla in turbid waters induced by the strong absorption of terrestrial material such as colored dissolved organic matter (CDOM) and detritus (He et al., 2013; Yamaguchi et al., 2012). In the cold upwelling areas (region A in Fig. 6b) in the southern TWS (Tang et al., 2002), chla concentrations are higher than in the surroundings. In contrast, in the Kuroshio region and the basin of the SCS, chla is very low with values of less than 0.25 μg/l due to the oligotrophic surface waters. It is worth noting that the chla is higher in the TWS, although the TWS obtains its water from the oligotrophic SCS and the Kuroshio in summer. We will now look at the chla changes with the intrusion of PRP as an example in 2008.

Before the intrusion of PRP, chla in the TWS was similar to the climatology distribution, as the image taken on 15 July 2008 in Fig. 7a shows. High chla value occurred near the coasts and in the upwelling areas in the southern TWS, whereas low chla values and clean water were located in the center of the middle and northern TWS (Fig. 5a). Due to the strong northward flow made up of clean oligotrophic waters from the SCS and the Kuroshio, chla was low in the Penghu Channel on 15 July 2008. However, with the intrusion of PPR (Fig. 5b–c), significant phytoplankton blooms occurred across the entire TWS (Fig. 7b–d), indicating that nutrients might be brought into the middle and northern TWS due to the intrusion of PRP combing with the runoffs from the small rivers in the TWS. It is unfortunate that the satellite images for 2008 are imperfect due to clouds, but the images do match the shipboard observations. Some of the better satellite images are presented and discussed in the following section, although there are no matching field data.

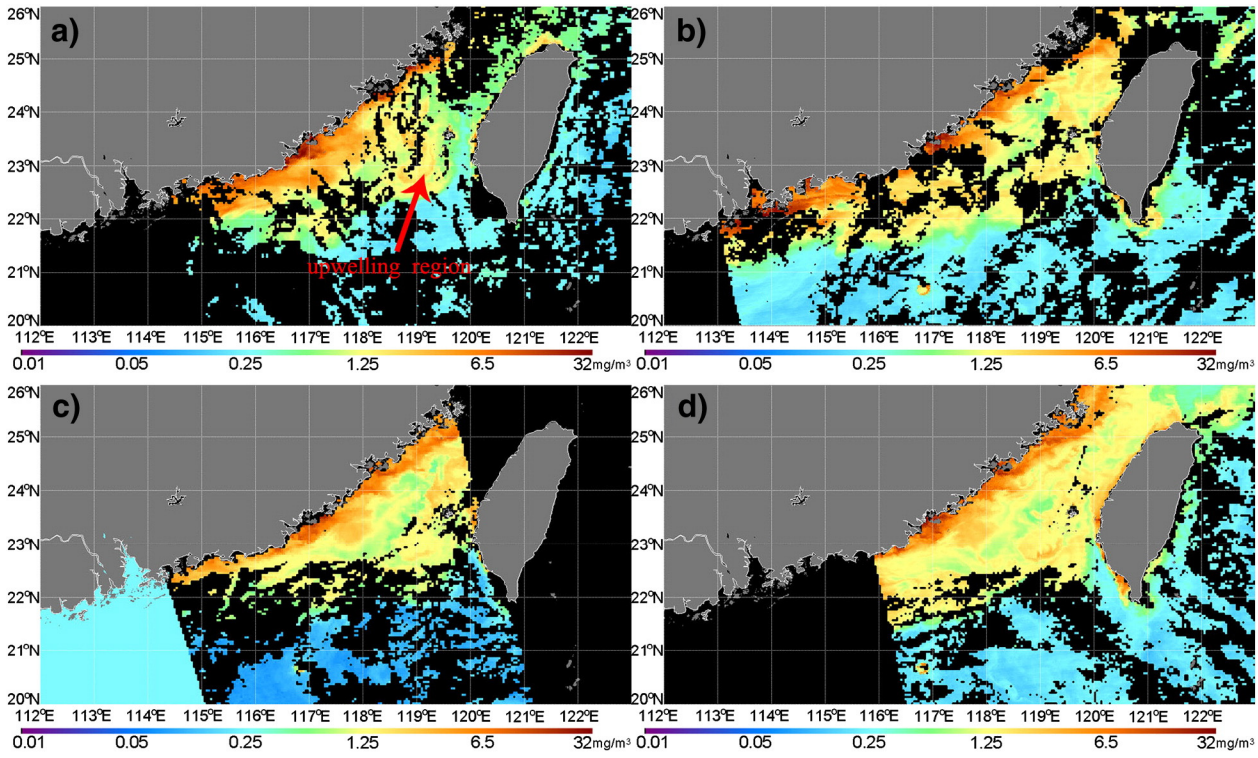


**Fig. 7.** chla images retrieved by MODIS before and after the intrusion of the PRP. The black regions in the images are covered by cloud or contaminated by sun-glint. (a) 15 July 2008; (b) 22 July 2008; (c) 23 July 2008; (d) 24 July 2008.

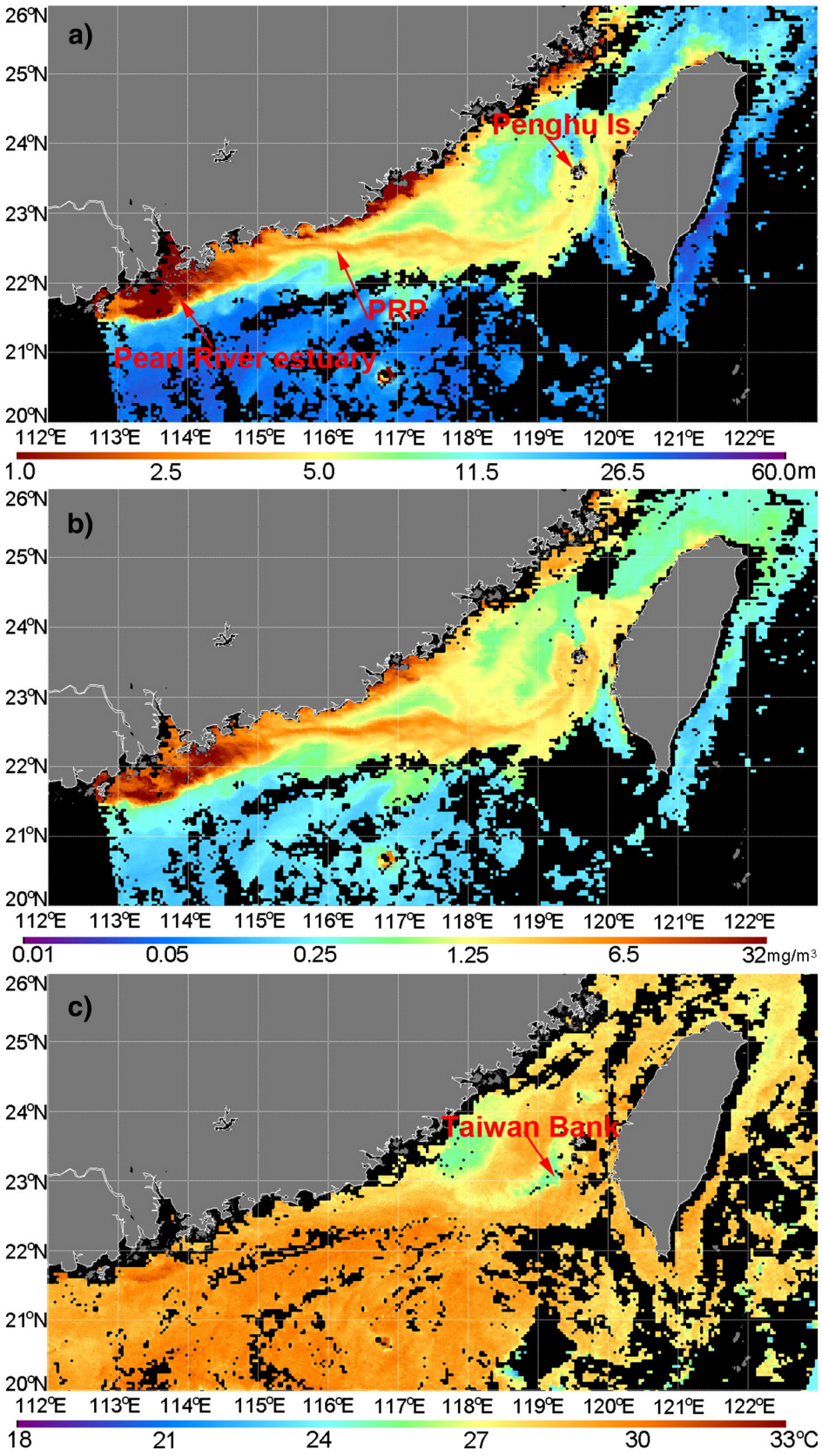


**Fig. 8.** Water transparency (a), chla (b) and SST (c) images on 9 July 2009. The black regions are covered by cloud or contaminated by sun-glint.

Important to point out is that although it is beyond the scope of this research there is no indication whether the nutrient supplied by the Pearl River is sufficient to sustain the phytoplankton bloom. Entrainment of subsurface, nutrient-rich water as the Pearl River plume spreads is perhaps also a significant source of nutrients (Chen, 2008).

### 3.3. Intrusion of the PRP into the Penghu Channel in other years

The intrusion of the PRP into the Penghu Channel in 2008 was not a unique event. Fig. 8 shows that the same event occurred in 2009, although we have no field data to validate the satellite remote sensing result. Both the water transparency and chla images on 9 July 2009 clearly show the PRP flowing eastwards like a narrow jet breaking away from the shore and passing the southern edge of the Taiwan Bank and into the Penghu Channel. The basic difference between the water transparency and chla images is that the water transparency shows the combined effects of the underwater light attenuation by terrestrial material and phytoplankton, whereas the chla reflects mainly phytoplankton. The low water transparency levels in the Pearl River estuary are caused by the runoff of turbid river water (Fig. 8a). The transparency then increases when the plume flows away from the estuary because the turbid freshwater is diluted by the clear seawater and the terrestrial particle material mostly settles. However, the maximum chla value occurs outside of the turbid estuary (Fig. 8b) where there is sufficient light for photosynthesis.

On the eastern side of the Taiwan Bank, the PRP turns to the northeast because of the strong northward flow in the Penghu Channel. It could be argued that the high chla values around the Taiwan Bank and Penghu Island are caused by upwelling, as the cold regions in Fig. 8c show. Upwelling may indeed bring rich nutrients up from the deep water to the upper layer and increase the chla value. However, the climatological distributions of chla and SST in the southern TWS in Fig. 6 show that high chla induced by upwelling is found only in the upwelling region south of Penghu Island. Further, a comparison of the positions of

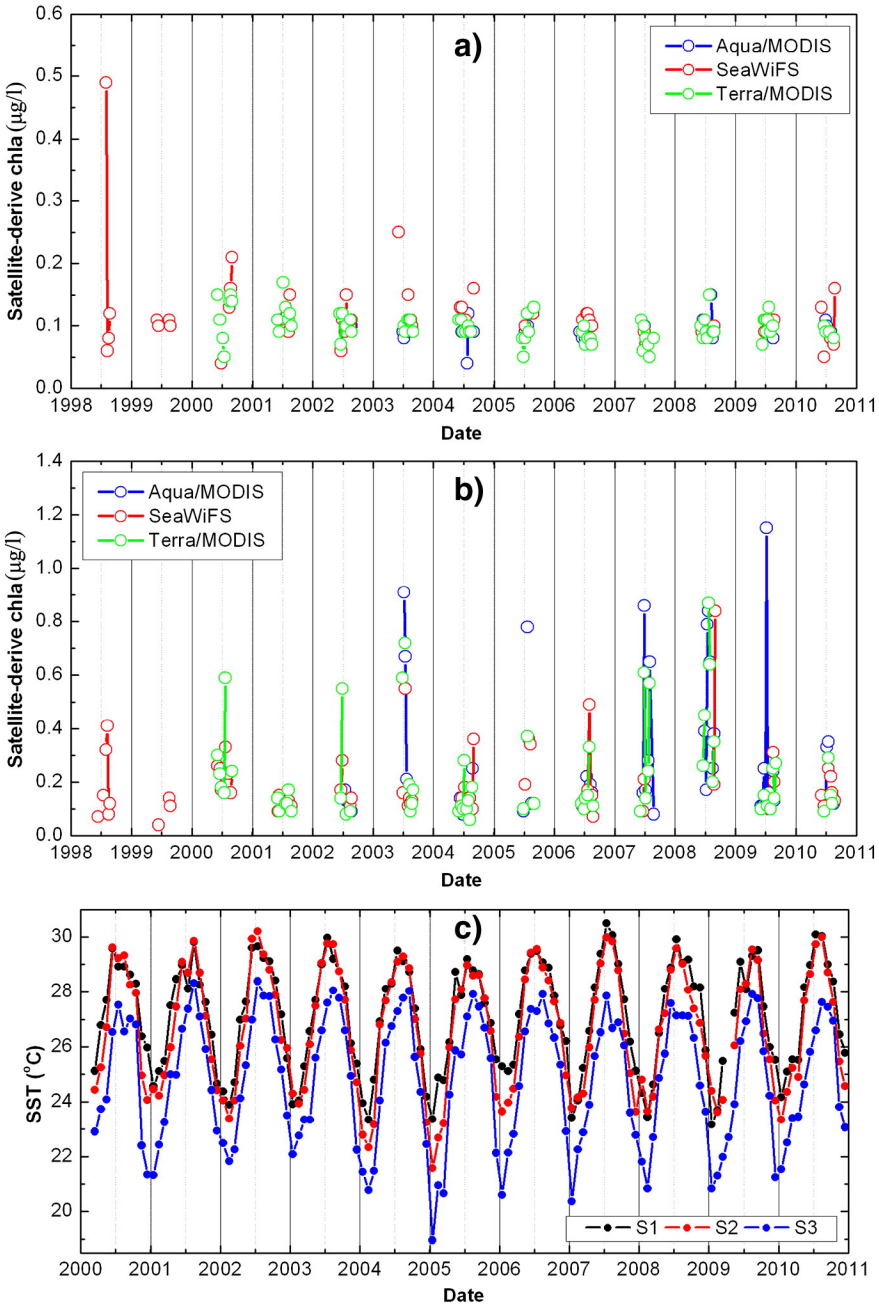


**Fig. 9.** Satellite-derive chla and SST at the three selected points (S1, S3 and S3) in Fig. 1. (a) 8-Day composite chla at point S1 during June–August from 1998 to 2010; (b) as in (a) but for point S2; (c) monthly mean SST at S1, S3 and S3 from 2000 to 2010.

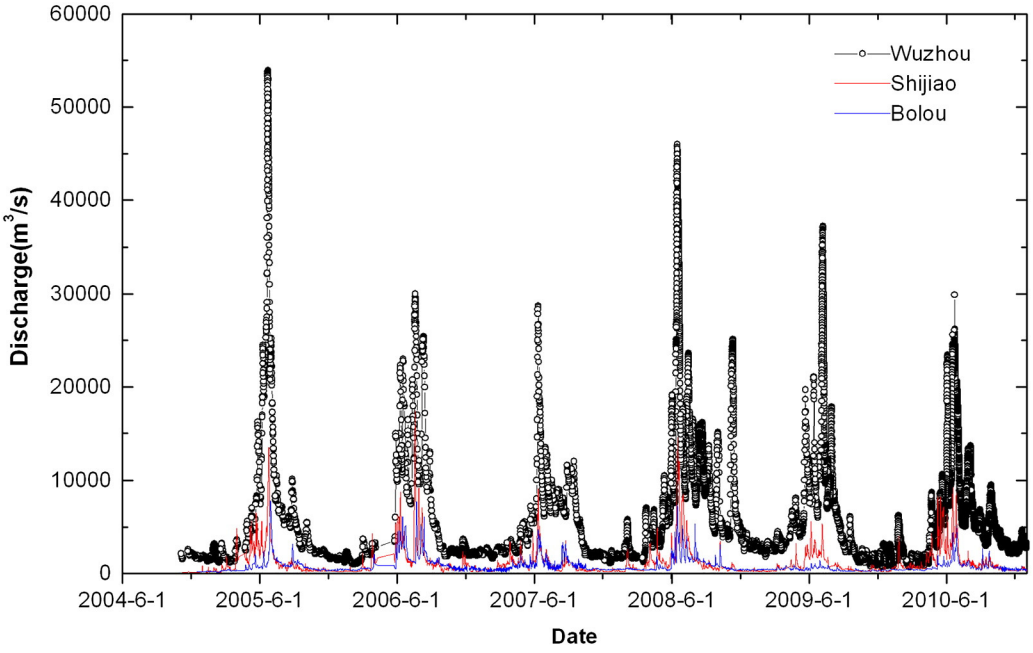


**Fig. 10.** Discharge of the three branches of the Pearl River. The Wuzhou, Shijiao and Bolou are the three hydrology stations that correspond to the west, north and east branches of the Pearl River, respectively.
Data are from the Hydrological Information Centre of China (http://xxfb.hydroinfo.gov.cn/).

the high chla and cold regions near the Taiwan Bank and Penghu Island reveals a high chla area (Fig. 8b) extending to the east of the cold upwelling region (Fig. 8c), indicating the intrusion of the PRP into the Penghu Channel.

Due to the heavy cloud coverage in the daily satellite images of water transparency and chla, it is difficult to establish a full map of the PRP in each year. To examine the intrusion of the PRP into the Penghu Channel during the summer in other years, we selected three representative points, S1 (119.50°E, 21.50°N), S2 (119.50°E, 22.60°N) and S3 (119.10°E, 23.00°N), as shown in Fig. 1. S1 is located in the basin of the SCS where the water depth is more than 2000 m, and is not affected by the PRP. S2 is located in the southwestern Penghu Channel where the water depth is about 200 m and is directly affected by the intrusion of the PRP, as revealed in Fig. 8. S3 is located at the upwelling region in the Taiwan Bank where the water depth is less than 25 m (Tang et al., 2002), as demonstrated by the climatology SST in Fig. 6b.

Fig. 9a and b shows the time series of the 8-day composite chla during June–August at points S1 and S2, respectively. In the basin of the SCS, as represented by point S1, chla is generally quite low with values of around 0.1 μg/l in summer. The episodic high chla in the summer of 1998 may be caused by a typhoon (Chen et al., 2012). However, the chla values at S2 are much higher than those at S1, indicating the addition of nutrients at S2. Generally, there are two possible sources of nutrients at S2: the PRP and upwelling.

Fig. 9c shows the time series of the monthly mean SST values from March 2002 to December 2010. Clearly, during summer, the SST values at S3 are about 2 °C lower than that at S1, which is consistent with the results of previous studies (Hu et al., 2003; Tang et al., 2002) that posit a strong upwelling in the Taiwan Bank. However, the SST values at S2 are almost the same as those at S1 during summer, indicating that S2 is not directly affected by upwelling. In addition, the strong northward flows in the Penghu Channel (Jan et al., 2002; Jan and Chao, 2003; Wu et al., 2007, see also Section 4.2) prevent the advection of nutrients and chla from the upwelling region around S3 to S2. The strong upwelling in 2010 and the weak upwelling in 2009 correspond to the low chla values in 2010 and the high chla in 2009, which supports the notion that upwelling in S2 is not the main controlling factor of the high chla values at S2. The source of nutrients that lead to the high chla values at S2 is more likely to be the intrusion of PRP. A comparison of the chla values at S2 and S1, as shown in Fig. 9a–b, shows that the intrusion of PRP into the Penghu Channel likely happens almost every year, although at different magnitudes. During the period 1998–2010, the intrusion in the summer of 2009 was the strongest, as revealed in Fig. 9b, but the intrusion was also quite strong in the summers of 2003, 2007 and 2008.

### 3.4. Factors controlling the intrusion of the PRP into the Penghu Channel

Many factors may affect the path of the PRP on the shelf in summer, including various oceanic dynamic forcings (wind, upwelling and basin-scale circulation), river discharge and the topography of the shelf (Ou et al., 2009). Of these various factors, river discharge and wind fields are the most variable (Ou et al., 2009), and thus may determine the occurrence of the intrusion of the PRP into the Penghu Channel.

We first examine the time series river discharges of Pearl River. Fig. 10 shows the river discharges at the Wuzhou, Shijiao and Boluo hydrological gauging stations from 4 November 2004 to 19 March, 2011, located in three main branches of the Pearl River, the Xi Jiang (West River), Bei Jiang (North River) and Dong Jiang (East River), respectively. The discharge in 2005, 2008 and 2009 was significantly larger than in other years. The significant intrusion of the PRP into the eastern TWS occurred in 2008 and 2009, which corresponds to large river discharges, but no significant intrusion can be identified in 2005 although the maximum river discharge occurred in this year. Variation in the wind field may better explain the intrusion events, thus, we will examine the sea surface wind vector data in the following.

We first show the 8-day mean chla images corresponding to the maximum PRP extension retrieved by Aqua/MODIS in the summers of 2005, 2008 and 2009 in Fig. 11a–c, and then present the 3-day merged sea surface wind vector images retrieved by QuikSCAT just before the chla images in Fig. 11d–f. Before the maximum PRP extension in the summers of 2008 and 2009, the northern SCS was dominated by strong southerly and southwesterly winds, which favor the eastward transport

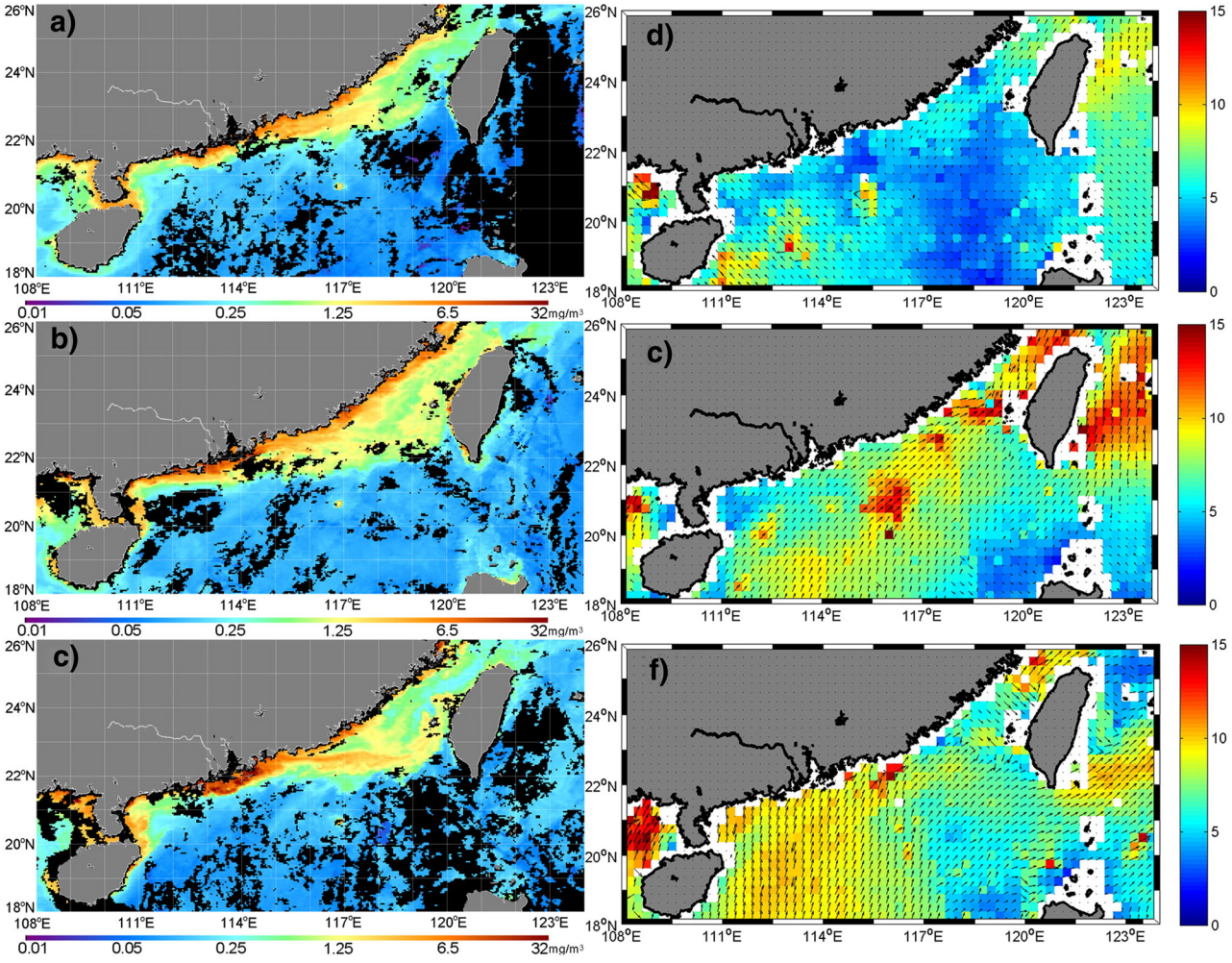


**Fig. 11.** Eight-day mean chla images corresponding to the maximum extension of the high chla retrieved by MODIS, and the 3-day merged sea surface wind vector (SSW) (m/s) images retrieved by QuikSCAT just before the chla images. (a) chla image between 12 and 19 July 2005; (b) chla image between 20 and 27 July 2008; (c) chla image between 4 and 11 July 2009; (d) SSW image between 9 and 11 July 2005; (e) SSW image between 17 and 19 July 2008; (f) SSW image between 1 and 3 July 2009.

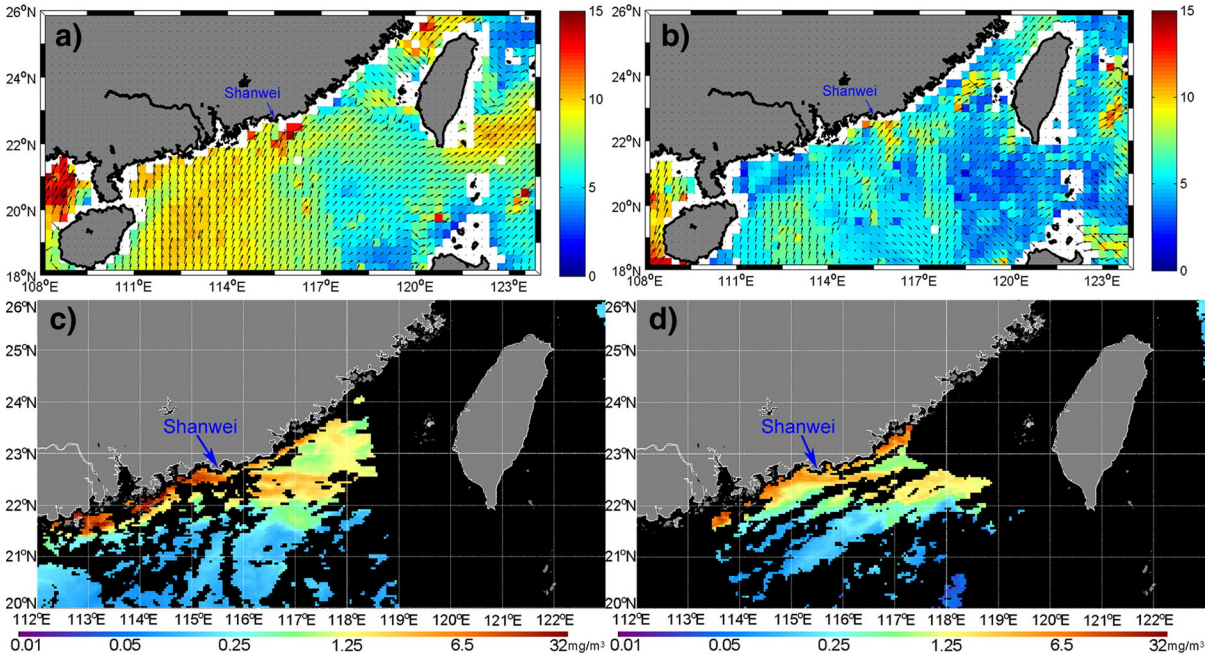


**Fig. 12.** Three-day merged sea surface wind vector (SSW) (m/s) and daily chla images retrieved by QuikSCAT and Aqua/MODIS. (a) SSW image between 1 and 3 July 2009; (b) SSW image between 4 and 6 July 2009; (c) chla image on 7 July 2009; (d) chla image on 8 July 2009.

of the PRP on the shelf of the northern SCS. A southwesterly wind also favors upwelling along the coasts of the northern SCS and the southern TWS, which may enhance the offshore detachment of the PRP. Based on a numerical model simulation, Gan et al. (2009) found that the PRP enhances the stratification and thins the surface frictional layer, which enhances the cross-shelf circulation in the upper water column such that the surface Ekman current and compensating flow beneath the plume are amplified. This effect may be important for the eastward transport of the PRP and its intrusion into the Penghu Channel in the summers of 2008 and 2009. However, before the maximum PRP extension in the summer of 2005, winds were weak on the shelf of the northern SCS and the directions of the wind vector were confused. Weak and confused winds are unfavorable for the eastward transport of the PRP, which may explain the weak intrusion of the PRP into the eastern TWS in the summer of 2005, despite this being the year of the highest river discharge.

The formation of the jet-shaped PRP in the summer of 2009 merits further discussion. Generally, driven by the climatological southwesterly winds in summer, the PRP forms a wide and deep buoyant plume over the shelf after leaving the estuary (Gan et al., 2009). At first order, winds may play an important role. Before the formation of the jet-shaped PRP, very strong southwesterly winds occurred near the coast of Shanwei with a maximum wind speed of up to 15 m/s, as shown in Fig. 12a–b. Such strong southwesterly winds lasted for about one week, which may have caused the rapid eastward transport of the PRP and the formation of the jet. Fig. 12c and d shows the daily chla images on the 7 July and 8 July 2009, respectively, just after the bursts of strong wind. Clearly, the jet-shaped PRP formed before 7 July and detached offshore near the coast of Shanwei, where the strong southwesterly winds occurred. Unfortunately, there are no valid satellite chla images taken during these strong winds because of cloud coverage, and we cannot judge the exact date of the formation of the jet.

To further validate the intrusion and its controlling factors, we use the numerical Seas Around Taiwan (SAT) model to simulate the flow fields. Fig. 13 shows the 6-day averaged flow fields at the surface layer during the periods 4 to 9 July 2005, 17 to 22 July 2008, 23 to 28 July 2008, 29 July to 4 August 2008, and 1–6 July 2009, which are just before the maximum extension of the high chla as retrieved by MODIS. The

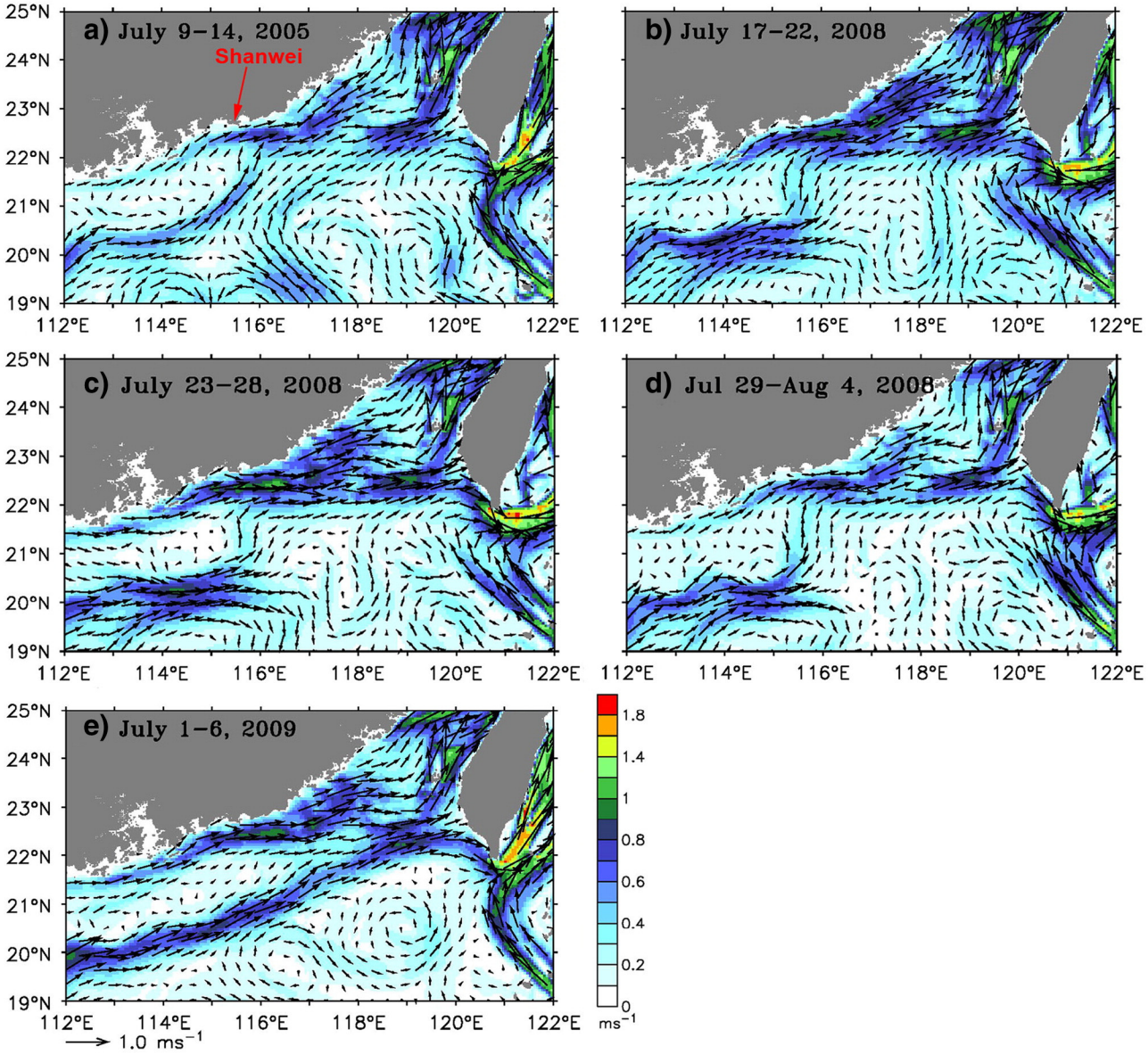


**Fig. 13.** Six-day average flow fields at the surface layer just before the maximum extension of the high chla retrieved by MODIS. (a) Flow fields during 4 to 9 July 2005; (b)–(d) flow fields during 17–22 July, 23–28 July and 29 Jul–4 Aug 2008, respectively; (e) Flow fields during 1 to 6 July 2009.

eastward flows along the Guangdong coast carried the Pearl River runoff firstly to Shanwei and then into the TWS, with part of the flows intruding into the Penghu Channel. Compared with the flows during July 2005, the eastward flows near Shanwei during July 2008 and July 2009 were much stronger, with a maximum velocity of up to 1 m/s. Due to the strong eastward flow near Shanwei, the intrusions of the PRP into the Penghu Channel in 2008 and 2009 were also much stronger than that in 2005, which is consistent with the satellite observations in Fig. 11a–c. In addition, the narrow and strong eastward flow near Shanwei in 2009 caused the jet-shape intrusion of the PRP into the Penghu Channel, as observed by the satellite images in Fig. 8.

Model-simulated trajectories of particles further support the intrusion of the PRP into the Penghu Channel. Fig. 14 shows the trajectories of particles released near Shanwei and the mouth of Pearl River on 9 July 2005, 17 July 2008 and 1 July 2009, corresponding to the period of simulated flow fields in Fig. 13. Compared with the trajectories of particles released on 9 July 2005, particles transported into the Penghu Channel in 2008 and 2009 were much stronger than that in 2005, which was consistent with the strong intrusions of the PRP into the Penghu Channel in 2008 and 2009 observed by the satellite.

## 4. Implications of the intrusion of the PRP into the Penghu Channel

River plumes are critical zones of land–ocean interaction where transformation takes place for the export of sediments, nutrients and organic material from land to the oceans (Cooley et al., 2007; Dagg et al., 2004; Dai et al., 2008). The PRP has high nutrient concentrations (silicate 130–140 μM, nitrate 75–100 μM and phosphate 0.2–1.2 μM)

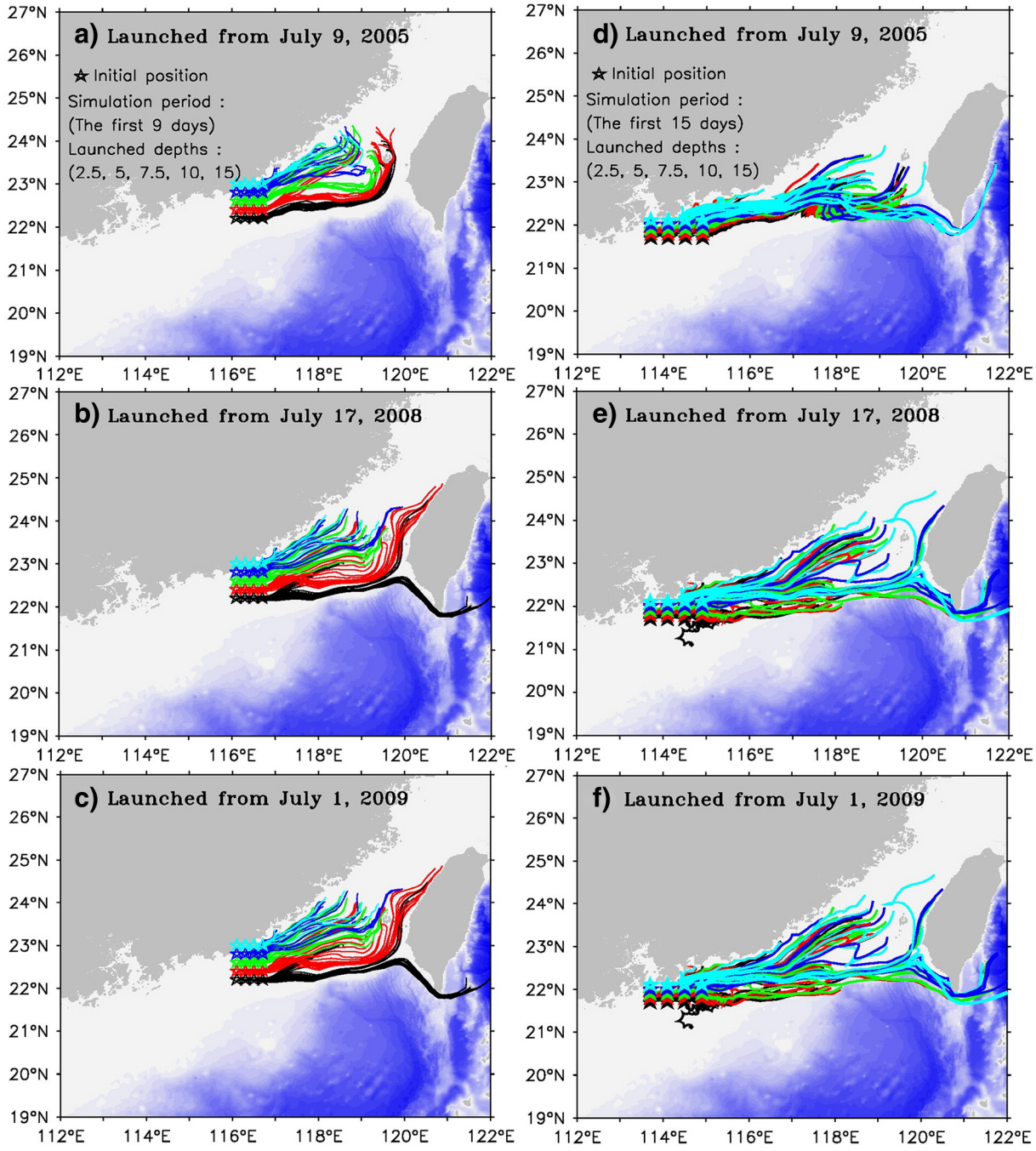


**Fig. 14.** Model-simulated trajectories of particles during the first 9 days after released near Shanwei (left), and during the first 15 days after released near the mouth of Peal River (right) with launched depths of 2.5 m, 5.0 m, 7.5 m, 10.0 m and 15.0 m. (a) and (d) launched from July 9, 2005; (b) and (e) launched from July 17, 2008; (c) and (f) launched from July 1, 2009.

and a high total dissolved inorganic carbon (DIC) (1500 μmol/kg) and TA (1200 μmol/kg) content at near-zero salinity in the Pearl River basin, which is widely covered by karst (Cai et al., 2004; Chen et al., 2008). In the wet season, with an average discharge of 16,000 $m^3$/s, the nutrients in the plume contribute about 70% of the total annual nutrient load and 80% of the total annual biomass in the shelf waters, and biological productivity is higher in the plume than in the upwelled water (Gan et al., 2010).

The flow through the Penghu Channel is much stronger than that through the western prong between mainland China and the Taiwan Bank (Fig. 13). The maximum velocity through the Penghu Channel is up to 1.2 m/s. Carried by the strong northward flow, the PRP intruding into the Penghu Channel is quickly transported to the middle and northern TWS and then enters the ECS. Thus, the intrusion of the PRP into the Penghu Channel may be important for understanding the nutrient dynamics and carbon budget in the ECS and SCS.

In addition, the northward flows in the TWS are generally parallel to the axis of the TWS, as shown in Fig. 13. Thus, the nutrients entering the ECS that are carried by the flows through the western prong between mainland China and the Taiwan Bank may be limited along the coasts of mainland China, whereas the nutrients carried through the Penghu Channel may be transported to the wide shelf of the ECS, where nutrients are quite limited in summer.

## 5. Conclusion

The large Pearl River discharge and strong southwesterly winds on the shelf are known to be responsible for the occurrence of the intrusion of the PRP into the western Taiwan Strait in summer. Our results have identified the intrusion of the PRP into the Penghu Channel in the eastern Taiwan Strait in the summers of 2008 and 2009 based on in situ measurements of the NTA and satellite remote sensing data. A significant phytoplankton bloom occurred across the entire TWS with an unusually strong intrusion of the PRP. Our results also reveal that the PRP intrudes into the Penghu Channel in the summer of most years. To the best of our knowledge, this study is the first time that the intrusion of the PRP into the Penghu Channel, the major channel connecting the East and South China Seas has been observed by satellite images and confirmed by modeling and field data.

Both satellite observations and the numerical model simulation showed a jet-shaped PRP intruding into the Penghu Channel in the summer of 2009, perhaps induced by the strong northward winds on the shelf of the northern SCS. However, the bottom topography, coast line, basin-scale circulation, eddies, internal wave and tides may also affect the PRP, and these factors deserve further study. Because of the high nutrient and DIC in the PRP and its fast transportation to the wide shelf of the ECS through the Penghu Channel, the intrusion of the PRP into the Penghu Channel may be important for understanding the nutrient dynamics and carbon exchange between the East and South China Seas.

## Acknowledgments

The authors would like to thank the crews of the R/V Ocean Researcher I for their help in field sampling. We thank the satellite data receiving station of the Second Institute of Oceanography (SIO/SOA) of China for providing the MODIS and AVHRR data. We also thank NASA for providing the chla, SST and SSW data sets. This study was supported by the National Key Technology Support Program of China (grants #2013BAD13B01 and #2012BAH32B01), the National Basic Research Program of China (grant #2009CB421202), the National Natural Science Foundation of China (grants #41322039, #41321004 and #41271378), and the "Global Change and Air–Sea Interaction" project of China (GASI-03-03-01-01). C.T.C acknowledges the support of the Ministry of Science and Technology of Taiwan (MOST 103-2611-M-110-010, NSC 101-2611-M-110-010-MY3) and the "Aim for the Top University" program (03c 0302 04). Y.C.H. thanks the support of the Ministry of Science and Technology of Taiwan (MOST 102-2611-M-001-001-MY2). J. van Beusekom and anonymous reviewers provided constructive comments which strengthened the manuscript.

## References

Brasse, S., Reimer, A., Seifert, R., Michaelis, W., 1999. The influence of intertidal mudflats on the dissolved inorganic carbon and total alkalinity distribution in the German Bight, southeastern North Sea. J. Sea Res. 42, 93–103.

Cai, W.J., Dai, M.H., Wang, Y.C., Zhai, W.D., Huang, T., Chen, S.T., Zhang, F., Chen, Z.Z., Wang, Z.H., 2004. The biogeochemistry of inorganic carbon and nutrients in the Pearl River estuary and the adjacent Northern South China Sea. Cont. Shelf Res. 24, 1301–1319.

Chen, C.T.A., 1993. Carbonate chemistry of the wintertime Bering Sea marginal ice zone. Cont. Shelf Res. 13 (1), 67–87. http://dx.doi.org/10.1016/0278-4343(93)90036-W.

Chen, C.T.A., 2002. Shelf- vs. dissolution-generated alkalinity above the chemical lysocline. Deep-Sea Res. II 49 (24–25), 5365–5375. http://dx.doi.org/10.1016/S0967-0645(02)00196-0.

Chen, C.T.A., 2008. Buoyancy leads to high productivity of the Changjiang Diluted Water: a note. Acta Oceanol. Sin. 27 (6), 133–140.

Chen, C.T.A., Millero, F.J., 1979. Gradual increase of oceanic $CO_2$. Nature 277 (5693), 205–206.

Chen, C.T.A., Pytkowicz, R.M., 1979. On the total $CO_2$–titration alkalinity–oxygen system in the Pacific Ocean. Nature 281 (5730), 362–365.

Chen, C.T.A., Sheu, D.D., 2006. Does the Taiwan Warm Current originate in the Taiwan Strait in wintertime? J. Geophys. Res. 111, C04005. http://dx.doi.org/10.1029/2005JC003281.

Chen, C.T.A., Wang, S.L., 1999. Carbon, alkalinity and nutrient budgets on the East China Sea continental shelf. J. Geophys. Res. 104 (C9), 20675–20686.

Chen, C.T.A., Wang, S.L., 2006. A salinity front in the southern East China Sea separating the Chinese coastal and Taiwan Strait waters from Kuroshio waters. Cont. Shelf Res. 26, 1636–1653.

Chen, H., Hu, J.Y., Pan, W.R., Zeng, G.N., Chen, Z.Z., He, Z.G., Zhang, C.Y., Li, H., 2002. Underway measurement of Sea Surface Temperature and Salinity in the Taiwan Strait in August, 1999. Mar. Sci. Bull. 4, 11–18.

Chen, C.T.A., Liu, C.T., Chuang, W.S., Yang, Y.J., Shiah, F.K., Tang, T.Y., Chung, S.W., 2003. Enhanced buoyancy and hence upwelling of subsurface Kuroshio waters after a typhoon in the southern East China Sea. J. Mar. Syst. 42, 65–79.

Chen, C.T.A., Hou, W.P., Gamo, T., Wang, S.L., 2006a. Carbonate-related parameters of subsurface waters in the West Philippine, South China and Sulu Seas. Mar. Chem. 99, 151–161.

Chen, C.T.A., Wang, S.L., Chou, W.C., Sheu, D.D., 2006b. Carbonate chemistry and projected future changes in pH and $CaCO_3$ saturation state of the South China Sea. Mar. Chem. 101, 277–305.

Chen, C.T.A., Wang, S.L., Lu, X.X., Zhang, S.R., Lui, H.K., Tseng, H.C., Wang, B.J., Huang, H.I., 2008. Hydrogeochemistry and greenhouse gases of the Pearl River, its estuary and beyond. Quat. Int. 186, 79–90.

Chen, X.Y., Pan, D.L., He, X.Q., Bai, Y., Wang, D.F., 2012. Upper ocean response to category 5 typhoon Megi in the western north Pacific. Acta Oceanol. Sin. 31, 51–58.

Clayton, T.D., Byrne, R.H., 1993. Spectrophotometric seawater pH measurements — total hydrogen-ion concentration scale calibration of m-cresol purple and at-sea results. Deep-Sea Res. I 40, 2115–2129.

Cooley, S.R., Coles, V.J., Subramaniam, Yager, P.L., 2007. Seasonal variations in the Amazon plume-related atmospheric carbon sink. Global Biogeochem. Cycles 21, GB3014. http://dx.doi.org/10.1029/2006GB002831.

Dagg, M., Benner, R., Lohrenz, S., Lawrence, D., 2004. Transformation of dissolved and particulate materials on continental shelves influenced by large rivers: plume processes. Cont. Shelf Res. 24, 833–858.

Dai, M.H., Zhai, W.D., Cai, W.J., Callahan, J., Huang, B.Q., Shang, S.L., Huang, T., Li, X.L., Lu, Z.M., Chen, W.F., Chen, Z.Z., 2008. Effects of an estuarine plume-associated bloom on the carbonate system in the lower reaches of the Pearl River estuary and the coastal zone of the northern South China Sea. Cont. Shelf Res. 28, 1416–1423.

Dong, L.X., Su, J.L., Wong, L.A., Cao, Z.Y., 2004. Seasonal variation and dynamics of the Pearl River plume. Cont. Shelf Res. 24, 1761–1777.

Friis, K., Körtzinger, A., Wallace, D.W.R., 2003. The salinity normalization of marine inorganic carbon chemistry data. Geophys. Res. Lett. 33 (2), 1085. http://dx.doi.org/10.1029/2002GL015898.

Gan, J.P., Li, L., Wang, D.X., Guo, X.G., 2009. Interaction of a river plume with coastal upwelling in the northeastern South China Sea. Cont. Shelf Res. 29, 728–740.

Gan, J.P., Lu, Z.M., Dai, M.H., Cheung, A.Y.Y., Liu, H.B., Harrison, P., 2010. Biological response to intensified upwelling and to a river plume in the northeastern South China Sea: a modeling study. J. Geophys. Res. 115, C09001. http://dx.doi.org/10.1029/2009JC005569.

Gran, G., 1952. Determination of the equivalence point in potentiometric titrations. Part II. Analyst 77, 661–671.

He, X.Q., Pan, D.L., Mao, Z.H., Zhu, Q.K., 2004. The study on the inversing model of water transparency using the SeaWiFS data. Acta Oceanol. Sin. 26 (5), 55–62.

He, X.Q., Bai, Y., Pan, D.L., Chen, C.T.A., Cheng, Q., Wang, D.F., Gong, F., 2013. Satellite views of the seasonal and interannual variability of phytoplankton blooms in the eastern China seas over the past 14 yr (1998–2011). Biogeosciences 10, 4721–4739.

He, X.Q., Bai, Y., Chen, C.T.A., Hsin, Y.-C., Wu, C.-R., Zhai, W.D., Liu, Z.L., Gong, F., 2014. Satellite views of the episodic terrestrial material transport to the southern Okinawa Trough driven by typhoon. J. Geophys. Res. Oceans 119. http://dx.doi.org/10.1002/2014JC009872.

Hong, H.S., Zheng, Q.A., Hu, J.Y., Chen, Z.Z., Li, C.Y., Jiang, Y.W., Wan, Z.W., 2009. Three-dimensional structure of a low salinity tongue in the southern Taiwan Strait observed in the summer of 2005. Acta Oceanol. Sin. 28, 1–7.

Hong, H.S., Chen, C.T.A., Jiang, Y.W., Lou, J.Y., Chen, Z.Z., Zhu, J., 2011a. Source water of two-pronged northward flow in the southern Taiwan Strait in summer. J. Oceanogr. 64 (5), 737–751.

Hong, H.S., Chai, F., Zhang, C.Y., Huang, B.Q., Jiang, Y.W., Hu, J.Y., 2011b. An overview of physical and biogeochemical processes and ecosystem dynamics in the Taiwan Strait. Cont. Shelf Res. 31, S3–S12.

Hsin, Y.-C., Wu, C.-R., Shaw, P.-T., 2008. Spatial and temporal variations of the Kuroshio East of Taiwan, 1982–2005: a numerical study. J. Geophys. Res. 113, C04002. http://dx.doi.org/10.1029/2007JC004485.

Hsin, Y.-C., Qu, T., Wu, C.-R., 2010. Intra-seasonal variation of the Kuroshio southeast of Taiwan and its possible forcing mechanism. Ocean Dyn. 60, 1293–1306.

Hsin, Y.-C., Wu, C.-R., Chao, S.-Y., 2012. An updated examination of the Luzon Strait transport. J. Geophys. Res. 117, C03002. http://dx.doi.org/10.1029/2011JC007714.

Hu, J.Y., Kawamura, H., Hong, H.S., Pan, W.R., 2003. A review of research on upwelling in the Taiwan Strait. Bull. Mar. Sci. 73 (3), 605–628.

Isobe, A., 1999. On the origin of the Tsushima warm current and its seasonality. Cont. Shelf Res. 19, 117–133.

Jan, S., Chao, S.Y., 2003. Seasonal variation of volume transport in the major inflow region of the Taiwan Strait: the Penghu Channel. Deep-Sea Res. II 50, 1117–1126.

Jan, S., Wang, J., Chern, C.S., Chao, S.Y., 2002. Seasonal variation of the circulation in the Taiwan Strait. J. Mar. Syst. 35, 249–268.

Jiao, N.Z., Zhang, Y., Zeng, Y.H., Gardner, W.D., Mishonov, A.V., Richardson, M.J., Hong, N., Pan, D.L., Yan, X.H., Jo, Y.H., Chen, C.T.A., Wang, P.X., Chen, Y.Y., Hong, H.S., Bai, Y., Chen, X.H., Huang, B.Q., Deng, H., Shi, Y., Yang, D.C., 2007. Ecological anomalies in the East China Sea: impacts of the Three Gorges Dam? Water Res. 41, 1287–1293.

Katoh, O., Morinaga, K., Nakagawa, N., 2000. Current distributions in the southern East China Sea in summer. J. Geophys. Res. 105 (C4), 8565–8573.

Lee, K., Tong, L.T., Millero, F.J., Sabine, C.L., Dickson, A.G., Goyet, C., Park, G.H., Wanninkhof, R., Feely, R.A., Key, R.M., 2006. Global relationships of total alkalinity with salinity and temperature in surface waters of the world's oceans. Geophys. Res. Lett. 33, L19605. http://dx.doi.org/10.1029/2006GL027207.

Liu, K.K., Tang, T.Y., Gong, G.C., Chen, L.Y., Shiah, F.K., 2000. Cross-shelf and along-shelf nutrient fluxes derived from flow fields and chemical hydrography observed in the southern East China Sea off northern Taiwan. Cont. Shelf Res. 20, 493–523.

Lou, J.Y., Chen, C.T.A., Lui, H.K., Selvaraj, K., Zhang, S.R., Lu, X.X., 2014. Comparison of subtropical surface water chemistry between the large Pearl River in China and small mountainous rivers in Taiwan. J. Asian Earth Sci. 79, 182–190.

Naik, H., Chen, C.T.A., 2008. Biogeochemical cycling in the Taiwan Strait. Estuar. Coast. Shelf Sci. 78, 603–612.

Ou, S.Y., Zhang, H., Wang, D.X., 2009. Dynamics of the buoyant plume off the Pearl River Estuary in summer. Environ. Fluid Mech. 9, 471–492.

Shu, Y.Q., Wang, D.X., Zhu, J., Peng, S.Q., 2011. The 4-D structure of upwelling and Pearl River plume in the northern South China Sea during summer 2008 revealed by a data assimilation model. Ocean Model. 36, 228–241.

Tang, D.L., Kester, D.R., Ni, I.H., Kawamura, H., Hong, H.S., 2002. Upwelling in the Taiwan Strait during the summer monsoon detected by satellite and shipboard measurements. Remote Sens. Environ. 83, 457–471.

Tseng, R.S., Shen, Y.T., 2003. Lagrangian observations of surface flow patterns in the vicinity of Taiwan. Deep-Sea Res. II 50, 1107–1115.

Wang, S.L., Chen, C.T.A., Hong, G.H., Chung, C.S., 2000. Carbon dioxide and related parameters in the East China Sea. Cont. Shelf Res. 20 (4–5), 525–544. http://dx.doi.org/10.1016/S0278-4343(99)00084-9.

Wu, C.-R., Hsin, Y.-C., 2005. Volume transport through the Taiwan Strait: a numerical study, Terrestrial. Atmos. Ocean. Sci. 16 (2), 377–391.

Wu, C.-R., Hsin, Y.-C., 2012. The forcing mechanism leading to the Kuroshio intrusion into the South China Sea. J. Geophys. Res. 117, C07015.

Wu, C.-R., Chao, S.-Y., Hsu, C., 2007. Transient, seasonal and interannual variability of the Taiwan Strait Current. J. Oceanogr. 63, 821–833.

Wu, C.-R., Lu, H.-F., Chao, S.-Y., 2008. A numerical study on the formation of upwelling off northeast Taiwan. J. Geophys. Res. 113, C08025.

Yamaguchi, H., Kim, H.C., Son, Y.B., Kim, S.W., Okamura, K., Kiyomoto, Y., Ishizaka, J., 2012. Seasonal and summer interannual variations of SeaWiFS chlorophyll a in the Yellow Sea and East China Sea. Prog. Oceanogr. 105, 22–29.

Yin, K.D., Zhang, J.L., Qian, P.Y., Jian, W.J., Huang, L.M., Chen, J.F., Wu, M.C.S., 2004. Effect of wind events on phytoplankton blooms in the Pearl River estuary during summer. Cont. Shelf Res. 24, 1909–1923.

Zhang, J., Yu, Z.G., Wang, J.T., Ren, J.L., Chen, H.T., Xiong, H., Dong, L.X., Xu, W.Y., 1999. The subtropical Zhujiang (Pearl River) Estuary: nutrient, trace species and their relationship to photosynthesis. Estuar. Coast. Shelf Sci. 49, 385–400.